MNHMT2013-22112

IMPROVED THERMAL TRANSFER EFFICIENCY FOR PLANAR SOLAR THERMOPHOTOVOLTAIC DEVICES

David M. Bierman, Andrej Lenert, Evelyn N. Wang
Device Research Lab
Department of Mechanical Engineering
Massachusetts Institute of Technology
Cambridge, MA, USA

ABSTRACT

Solar thermophotovoltaic (STPV) devices provide conversion of solar energy to electrical energy through the use of an intermediate absorber/emitter module, which converts the broad solar spectrum to a tailored spectrum that is emitted towards a photovoltaic cell [1]. While the use of an absorber/emitter device could potentially overcome the Shockley-Queisser limit of photovoltaic conversion [2], it also increases the number of heat loss mechanisms. One of the most prohibitive aspects of STPV conversion is the thermal transfer efficiency, which is a measure of how well solar energy is delivered to the emitter. Although reported thermophotovoltaic efficiencies (thermal to electric) have exceeded 10% [3], [4], previously measured STPV conversion efficiencies are below 1% [5], [6], [7].

In this work, we present the design and characterization of a nanostructured absorber for use in a planar STPV device with a high emitter-to-absorber area ratio. We used a process for spatially-selective growth of vertically aligned multi-walled carbon nanotube (MWCNT) forests on highly reflective, smooth tungsten (W) surfaces. We implemented these MWCNT/W absorbers in a TPV system with a one-dimensional photonic crystal emitter, which was spectrally paired with a low bandgap PV cell. A high fidelity, system-level model of the radiative transfer in the device was experimentally validated and used to optimize the absorber surface geometry. For an operating temperature of approximately 1200 K, we experimentally demonstrated a 100% increase in overall STPV efficiency using a 4 to 1 emitter-to-absorber area ratio (relative to a 1 to 1 area ratio), due to improved thermal transfer efficiency. By further increasing the solar concentration incident on the absorber surface, increased emitter-to-absorber area ratios will improve both thermal transfer and overall efficiencies for these planar devices.

1. INTRODUCTION

Thermophotovoltaic (TPV) conversion is a method to convert thermal energy into work (or electrical energy) and, like other heat engines, is ultimately limited by the Carnot efficiency. In a TPV device, thermal emission takes place at the emitter and is directed towards a photovoltaic (PV) cell where the photon energy is converted to electrical energy. By introducing spectral control, TPV devices should deliver only photons useful for electrical conversion, *i.e.* photons with energy levels higher than that of the band-gap of the PV cell. This strategy can be accomplished in many ways such as the use of an optical filter between the emitter and the PV cell, or a back surface reflector located behind the PV cell [8].

Recently, researchers have investigated the use of 1-D and 2-D photonic crystals (1D, 2D PhC) to introduce selective emitters for the narrow band emission required in these devices by controlling the photon density of states [9], [10]. In all of these strategies *i.e.*, filter, reflector, PhC, sub-bandgap energy photons are utilized to maintain the temperature of the emitting device either through their recycling or suppressed emission. Thermal to electric TPV conversion has been reported as high as 19% [3].

Heat can be delivered to TPV devices in a number of ways, including (but not limited to) the combustion of fossil fuels [11], nuclear fission reactions [12], or concentrated solar power (CSP) [7]. The challenge in all of these cases is how to efficiently deliver this heat to the TPV conversion process. The latter strategy (using CSP) is known as solar thermophotovoltaic (STPV) conversion, and its efficiency relative to other strategies is largely characterized by what we will refer to as the thermal transfer efficiency. For a STPV device, thermal transfer efficiency is primarily a measure of the device's ability to absorb radiation, and suppress undesirable thermal re-emission from the same surface.

In this work, we designed, built and characterized a nanostructured solar absorber for a planar STPV device. We introduce a method to decouple the absorber area from the emitter area in order to improve the thermal transfer efficiency using a spatially-selective growth process of highly absorptive MWCNTs. The advantage is gained when high solar concentrations are available for the same absorber temperature. This strategy has been identified as a crucial design consideration for efficient performance of STPV systems [1], [13], but practical implementations have not been studied. Additionally, a high fidelity, system-level model is developed, experimentally validated, and used to aid in the fabrication of an optimized absorber geometry. We show a 100% improvement of this optimized device relative to a planar device whose absorber and emitter areas are equal. We report a 2.6% overall efficiency which more than doubles previously documented values. The dramatic improvement in thermal transfer efficiency demonstrated in this study represents a major step towards efficient STPV conversion.

2. NOMENCLATURE

AR	Area ratio of the emitter to the absorber surfaces [--]
g_2	Gap between shield and absorber [μm]
g_1	Gap between emitter and PV cell [μm]
MPP	Maximum power point [W]
$J_{i,\lambda}$	Spectral radiosity for surface i [W/m^2]
$E_{b,\lambda,I}$	Spectral blackbody emissive power for surface i [W/m^2]
$\varepsilon_{\lambda,i}$	Spectral emissivity for surface i [--]
$H_{\lambda,i}$	Spectral irradiance for surface i [W/m^2]
F_{i-j}	Diffuse view factor from surface i to j [--]
I_{photo}	Photocurrent generated at the PV cell [A]
A_{cell}	Active area of the PV cell [m^2]
e	Charge of an electron [C]
λ	Wavelength [μm]
h	Planck's constant [m^2-kg/s]
c_0	Speed of light in a vacuum [m/s]
IQE_λ	Spectral internal quantum efficiency [--]
$q_{em\text{-}cell,\lambda}$	Spectral heat flux incident on PV cell [W/m^2]
η_{stpv}	STPV efficiency [--]
$\dot{Q}_{solar}$	Solar power passing through aperture [W]
η_{abs}	Absorber efficiency [--]
$\bar{\alpha}$	Solar weighted absorptance [--]
$\bar{\varepsilon}$	Total hemispherical emissitance [--]
σ	Stefan-Boltzmann constant [W/m^2-K^4]
T	Temperature of absorber/emitter pair [K]
C	Solar concentration factor [--]
G_s	Solar flux [W/m^2]

3. ABSORBER DESIGN AND FABRICATION

For a planar STPV device, decoupling the absorber and the emitter areas can be accomplished simply by shrinking the absorber surface relative to the emitter surface. This absorbing surface was chosen to be MWCNTs for their high solar absorption and spectrally independent emissivity (for simplicity) [14]. By reducing the area of the absorbing surface, an inactive surface is exposed which does not participate in solar absorption, but is still able to lose heat via thermal re-emission. This surface was metallized in order to reduce this parasitic loss.
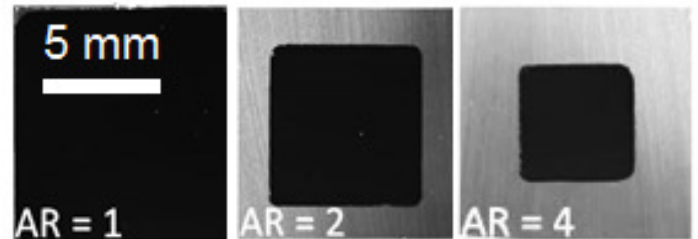

Figure 1: Top-down view of absorbing side of fabricated planar STPV device. The dark region is MWCNTs while the light region is the smooth W inactive region.

The absorber was fabricated using conventional physical and chemical vapor deposition (PVD, CVD) processes. A 200 nm tungsten (W) layer was sputtered on a 10 nm adhesion layer of titanium (Ti) which was deposited on the Si/SiO$_2$ substrate. This is the inactive metallized surface. Using a laser cut acrylic contact mask, a seed layer for MWCNT growth was then selectively deposited on to the samples with electron-beam evaporation.

The MWCNTs were grown using a CVD process in a H$_2$/He environment at elevated temperatures. This temperature of 720° C was reached within approximately 10 minutes and was then held constant for 5 minutes in order to anneal the Fe seed layer. Next, the carbon source (ethylene gas) was introduced to the furnace and MWCNTs were grown for 10 minutes. When growth was complete, the furnace was rapidly cooled. As shown in figure 1, the samples have a distinct black-body absorbing area and a low-emissivity non-absorbing area.

4. EXPERIMENTAL SETUP

This study focuses on the effect of the area of the emitter relative to the area of the absorber. To this end, we varied the emitter-to-absorber area ratio (AR) using the previously discussed fabrication method.

Figure 2 shows a schematic of the experimental setup used in this study. This setup provides minimal parasitic heat loss *i.e.*, conduction through supports, which allows the radiative transfer processes to dominate in this vacuum setting, offering a
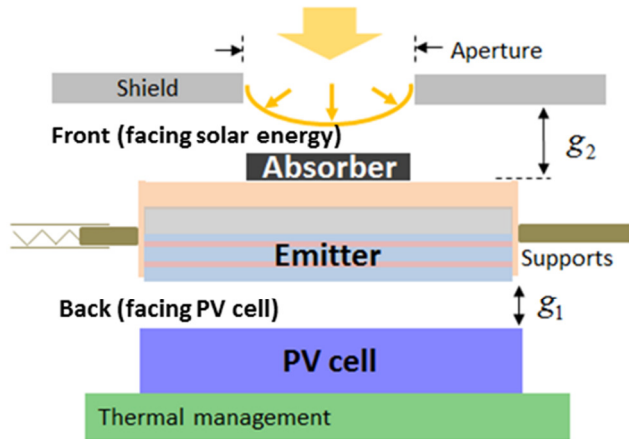
Copyright © 2013 by ASME

Figure 2: Schematic of planar STPV experiment. Measurement capabilities include incident solar radiation, output electrical work, temperature of absorber/emitter pair, and waste heat from the cell.

better understanding of the device performance. With this experimental design we are able to measure *in-situ* current-voltage (I-V) characterizations of the PV cell, thermal load on the PV cell, and incident solar power.

The samples were suspended using two hypodermic needles (*27Gx1.25", B-D*) and one spring loaded pin (*POGO-72U-S, ECT*). A small (~ 300 μm) gap, indicated as g_1 in figure 2, was then introduced between the emitter surface and the PV cell. In general, this gap is to be as small as possible for improved view factor to the cell. Next, a polished Al shield (*mirror-finish aluminum, McMaster-Carr*) was installed which had an aperture area equal to that of the MWCNTs. The shield was kept approximately 400 μm from the sample (g_2) in figure 2. The entire rig was put into a vacuum chamber and the pressure was reduced to 2 mT before testing began. This pressure is sufficiently low to suppress conduction through the air.

Solar radiation was simulated with a Xenon arc lamp (*92192, Newport Oriel Inc.*). The optical setup includes both imaging and non-imaging optical concentration components. The imaging concentration is achieved with a focusing lens / condenser stage (*Hi Flux Beam Concentrator, Newport*). The non-imaging concentration is achieved using a converging frustum light pipe with highly reflective, silver walls. These components allow for a range of solar concentrations between 3 and 37 W/cm^2. All of the power measurements were made with a thermopile radiation detector (*919P-040-50, Newport Oriel Inc.*).

The PV cell in the experiment was an InGaAsSb semiconductor which has a bandgap of 0.55 eV. The 1D PhC which was used consists of five alternating sub-wavelength layers of Si and SiO$_2$ with thicknesses of 255 and 490 nm, respectively. This provides a sharp cutoff wavelength around 2.3 μm – the bandgap energy of the PV cell used in the experiment– with a relatively easy fabrication process and

high-temperature material stability [11], [15]. The spectral emissivity as well as *IQE* of the photovoltaic cell can be found in [11].

The PV cell was kept near 20° C by flowing chilled water across its back-side. This water carries away the waste heat generated from the conversion process. We measure this waste heat using thermocouple readings of the water before and after thermal contact with the substrate of the PV cell, as well as the flow-rate of the chilled water loop (*L-5LPM-D, Alicat Scientific*).

A range of *AR* samples between 1 and 5 were tested. For each test, the amount of input power was varied while the PV cell and surrounding temperatures were held constant. Once steady state operation was reached, an *in situ* current-voltage (I-V) sweep was acquired (*2440, Keithley Instruments Inc.*) in order to determine the short circuit current, open circuit voltage, and maximum power point (*MPP*).

5. MODEL FORMULATION

In parallel with the experiments, a system level model was developed in order to predict the performance of the planar STPV device. The following assumptions were made in the formulation of the model: 1) Isothermal operation of the device 2) Diffuse emission and reflection at every surface, and 3) Diffuse input power source (i.e., the light coming through the aperture is split between the blackbody absorber and the low emissivity metal through their respective view factors). The last assumption was made due to the non-collimated light which undergoes multiple reflections in the converging light pipe [16].

Once the temperature of the absorber-emitter pair was specified, both radiative and conductive heat transfer with the surrounding components (PV cell, aperture shield, supports, vacuum chamber, etc.) can be determined. The radiative transfer was solved on a spectral basis via an energy balance at each surface in the network. For diffuse emission and reflection, the radiosity, $J_{\lambda i}$, is the sum of the thermal emission and the reflection of the irradiance:

$$J_{\lambda_i} = \varepsilon_{\lambda_i} E_{b\lambda_i} + (1 - \varepsilon_{\lambda_i}) H_{\lambda_i} \qquad (1)$$

The irradiance, $H_{\lambda i}$, is the portion of the radiosity from other surfaces in the network which is intercepted by the surface of interest. The intercepted portion is determined using diffuse view factors:

$$H_{\lambda_i} = \sum_{j=1}^{n} J_{\lambda_j} F_{ij} \qquad (2)$$

Because these equations are solved on a spectral basis, the total radiative heat transfer to each component is found through integration. Conduction losses from the mechanical supports were estimated using a fin approximation, justified by the small Biot number (<<0.1).

The sum of the radiative emission (both parasitic and useful) and heat conduction is the total heat that must be supplied to

3

Copyright © 2013 by ASME

the device to maintain the specified equilibrium temperature. This is used to determine the input power to the device.

To determine the output power of the device, we solve for the total radiative heat transfer from the emitter to the PV cell for energy levels higher than the PV cell (E_g = 0.55 eV). This useful radiation generates photocurrent based on the following expression:

$$I_{photo} = A_{cell} \int_0^\infty \frac{-e\lambda}{hc_0} IQE_\lambda \, q_{em-cell,\lambda} d\lambda \qquad (3)$$

Once the photocurrent is determined, we use empirical information from the PV cell used in the experiments to correlate this to the *MPP*.

6. RESULTS & DISCUSSION

Figure 3 shows typical acquired I-V sweeps from the experiments to characterize the diode response of the PV cell. These sweeps provide information about the short-circuit current, open-circuit voltage, maximum power point (*MPP*), and fill factor fill factor. Shown in the figure are the results for *AR*1 and *AR*4 under the maximum solar concentration of our experimental setup (373 kW/m^2). The higher currents generated in the *AR*1 device are a result of its higher operating temperatures for the same input heat flux.

The photocurrent that is calculated in the model is physically represented by the short-circuit current that we obtain from the I-V sweeps. Figure 4 shows both measured and predicted (solid lines) values of the short circuit current as a function of input solar concentration for different *AR*s. Since the model can describe the generated photocurrent of the cell as a function of solar concentration without any fitting parameters, the agreement between the predicted and measured short circuit current provides sufficient model validation and allows us to use the model to further explore the physics of the experiment.
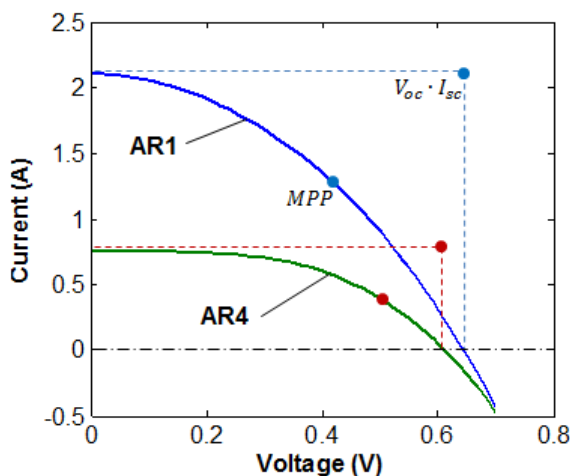

Figure 3: *In-situ* **I-V characterization of the InGaAsSb PV cell for AR1 and AR4 samples. The lower currents of AR4 reduce the effect of the series resistance in the diode circuit.**
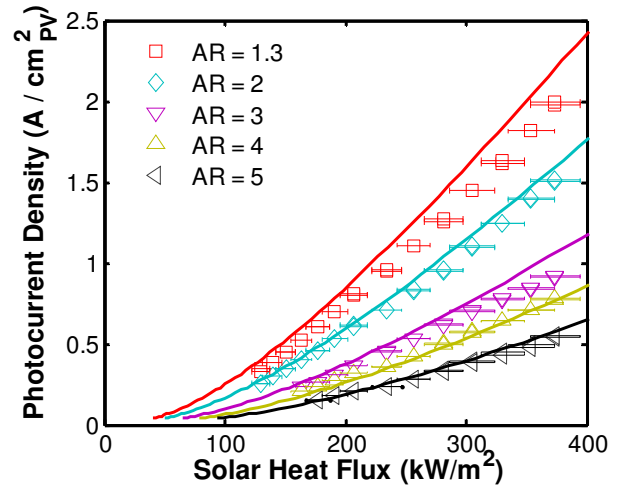

Figure 4: Generated photocurrent as a function of input heat flux to the absorber for a variety of AR.

Measured circuit quantities such as the shunt resistance, series resistance, and diode behavior allow us to construct an equivalent circuit model in order to relate the measured short-circuit current to the *MPP* which defines the output power of the device.

With information about the *MPP*, we can characterize the performance of our device once our input power is quantified. This input power is defined by the concentrated solar heat flux that passes through the aperture and is incident on the absorbing surface. This is simply the product of the measured concentrated heat flux and the aperture area, and is named $\dot{Q}_{solar}$. Next, we define STPV efficiency (η_{stpv}) as the ratio of output electrical power to input concentrated solar radiation. Note that this figure of merit does not include the optical efficiency which characterizes the performance of concentrating solar power.

$$\eta_{stpv} = \frac{MPP}{\dot{Q}_{solar}} \qquad (4)$$

For a fixed solar concentration, it was observed that relative to the *AR*1 sample, the STPV efficiency can be improved through an increase in *AR*. This improvement will reach an optimum value before the performance will begin to decrease. The optimum emerges because of the competing effects of TPV efficiency (thermal to electric) and thermal transfer efficiency (solar to thermal), and thus it is a function of solar concentration. In other words, while reducing the absorber area improves the efficiency by which heat is delivered to the emitter, it also decreases the input power to the device and therefore the temperature. As the temperature drops significantly below the optimum TPV temperature (1300 K), the emitter performance suffers. Figure 5 shows this phenomenon at a solar concentration of 354 kW/m^2.

The existence of an optimum geometry implies that for a given solar concentration, an STPV device should be designed with the appropriate AR in mind to maximize performance. It is notable that while the $AR5$ device had a steady-state temperature that was more than 300 K below that of the $AR1$ device at this particular concentration, its overall efficiency was over 50% better, highlighting the importance of thermal transfer efficiency.

Figure 6 shows the overall STPV conversion efficiency as a function of AR for a given output power, which corresponds to a fixed absorber/emitter pair temperature. The output power in figure 6 is 220 ± 15 mW which indicates an equilibrium temperature of approximately 1200 K. Note that this is 100 K lower than the optimum TPV temperature due to experimental limitations. By fixing the TPV performance at this temperature, this figure allows us to characterize the improvement in thermal transfer efficiency as a result of shrinking the absorber area.
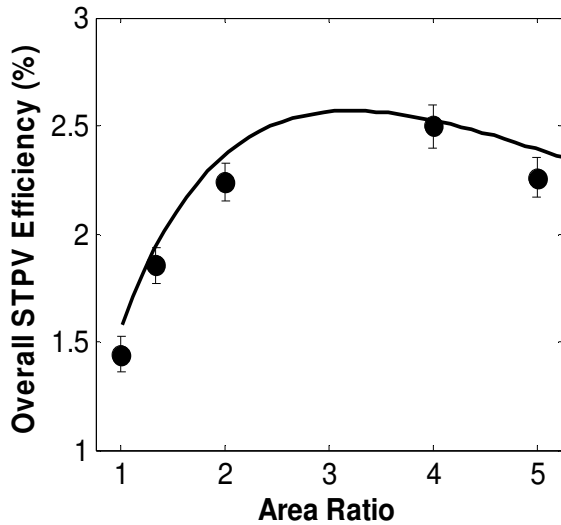

Figure 5: STPV efficiency as a function of emitter-to-absorber area ratios for a fixed solar concentration of 354 kW/m^2.

Consider the following expression for absorber performance:

$$\eta_{abs} = \bar{\alpha} - \frac{\bar{\varepsilon}\sigma T^4}{C G_s} \qquad (5)$$

For a blackbody surface ($\bar{\alpha} = \bar{\varepsilon} = 1$), this expression is simply a comparison between the emissive power of the surface to the concentration of the impinging radiation. Figure 6 essentially shows what happens when a higher solar concentration is used to reach the same temperature. We do this by modifying the geometry of the front of the device (varying AR), and thus altering the resultant energy balance. We are effectively trading a highly emissive surface (MWCNT) with a minimally emissive surface (W), and by increasing the solar concentration, we ensure that sufficient temperatures are reached. However, by reducing emissive loss at the front of the device, a smaller input power is required, which is manifested in the improved overall efficiency.
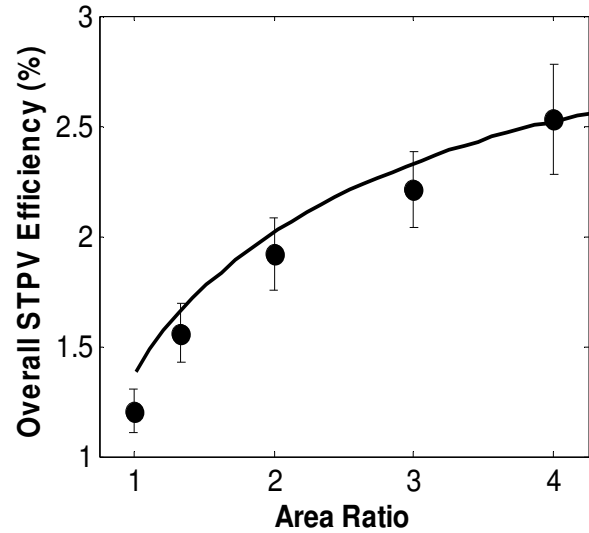

Figure 6: STPV efficiency for an absorber/emitter pair temperature of approximately 1200 K, showing the effect of increasing the solar concentration.

Assuming optimum TPV temperature could be reached (1300 K), the model was used to identify the key losses in the system. Figure 7 shows the results of a loss analysis of this planar design. The losses are reported as a percentage of the total input power. The first loss is the thermal re-emission due to the high emissivity CNT absorber surface. As AR increases to sufficiently high values, this contribution becomes negligible. This effect dramatically improves the thermal transfer efficiency even at relatively low ARs (2-4). The next loss is the inactive loss, defined here as the combined radiative heat transfer from the inactive front and side surfaces and conduction losses through the supports (between 5 and 10% of the input energy). The energy which remains after these losses is considered to be the heat delivered to the 1D PhC emitter, and it is therefore referred to as the thermal transfer efficiency. Using the model, we estimate a 100% improvement in thermal transfer efficiency as we shrink the area of the absorber to ¼ of the emitter area ($AR4$).

From a first order perspective, the ability to deliver thermal power to the TPV converter with a planar STPV device is ultimately limited by the non-zero emission from the front-side metallic surface. There are also higher order considerations as large ARs are considered, such as the effect of non-isothermal conditions and impractical solar concentrations, both of which will ultimately reduce the device performance.

As mentioned, we metallized our Si substrate with W in order to reduce the parasitic emissive losses in the system. At high ARs, the low-emissivity of this non-active surface is quite important. Figure 8 shows the effect of this surface on the performance of the planar STPV device at $AR4$. Also shown in the figure are lines of constant conversion efficiency. The metallization the surface improves the conversion efficiency of the device by approximately 1%, which is a nearly 100% relative increase from a black surface.

5   Copyright © 2013 by ASME
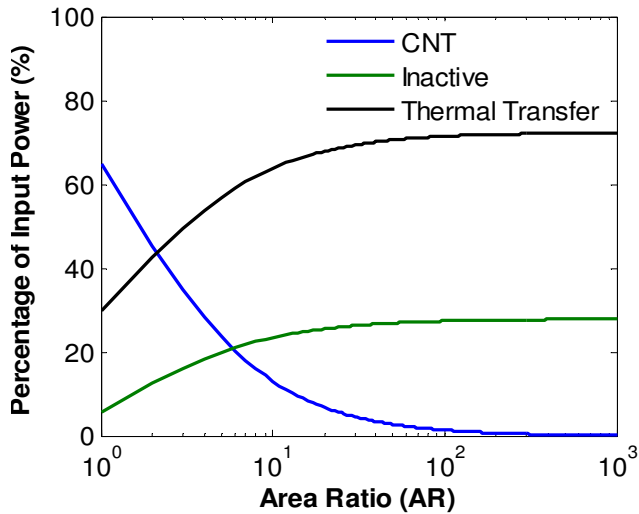
Figure 7: Results from a loss analysis of the planar STPV device showing which shows the thermal transfer efficiency asymptotically approaching 72%. These values are for an optimum TPV temperature of 1300 K.

The figure also indicates that if this surface were non-emitting *i.e.*, ε = 0, another 30% relative improvement could be reached and conversion efficiencies would exceed 3%. The inactive metallic area is unavoidable, however, for this planar design.

In figure 7, the AR10^3 case still has 30% of input heat not delivered to the TPV system, the asymptotic limit of this design. One way to achieve performance closer to the red line in figure 8 while still maintaining high AR is to re-configure the planar design into a cavity absorber whose aperture behaves as a blackbody absorber, and outer walls selectively emit radiation towards a photovoltaic jacket. This design eliminates the inactive area for parasitic thermal radiation. Our model was adapted to give an estimate of the performance of such a device. For an AR5 cavity design, STPV efficiencies
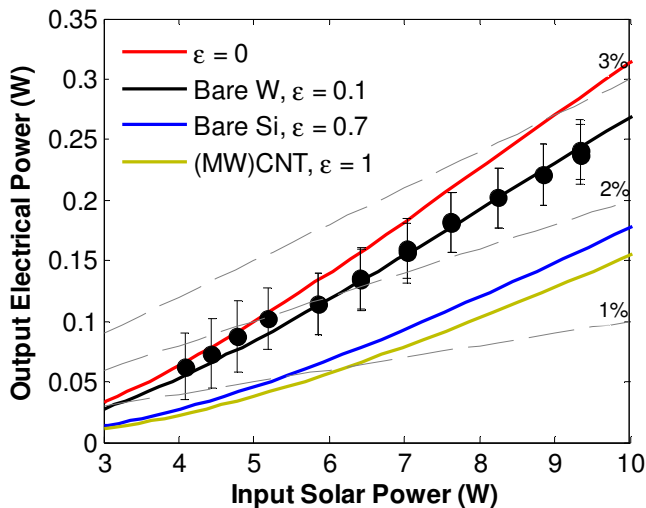

Figure 8: The effect of the inactive area on the STPV performance. Also shown are lines of constant STPV efficiency (dashed).

approaching 6% may be reached in the near term *i.e.*, using the same components used in this study, assuming that 10% of the absorbed radiation will be lost due to conduction and that the cavity walls remain isothermal. This efficiency could be reached at relatively modest solar concentrations (~600 kW/m^2).

7. CONCLUSION

In this work, we have presented a nanostructured absorber design which was fabricated and implemented into a planar STPV device. Through a spatially selective growth of MWCNT absorbers, we demonstrated that the de-coupling of absorber and emitter areas allowed us to improve thermal transfer and thus the overall efficiency by approximately 100% at a given temperature. We provide design considerations for planar STPV devices, as well as a discussion of the potential improvements gained from alternative geometries. This study represents an important step in the understanding of thermal transfer efficiency and its integral role in efficient STPV conversion.

REFERENCES

[1] N.-P. Harder and P. Wurfel, "Theoretical limits of thermophotovoltaic solar energy conversion," *Semiconductor Science and Technology*, vol. 18, no. 5, pp. S151–S157, May 2003.

[2] W. Shockley and H. J. Queisser, "Detailed Balance Limit of Efficiency of p-n Junction Solar Cells," *Journal of Applied Physics*, vol. 32, no. 3, p. 510, 1961.

[3] C. J. Crowley, "Thermophotovoltaic Converter Performance for Radioisotope Power Systems," in *AIP Conference Proceedings*, 2005, vol. 746, no. 1, pp. 601–614.

[4] P. F. Baldasaro, E. J. Brown, D. M. Depoy, B. C. Campbell, and J. R. Parrington, "Experimental assessment of low temperature voltaic energy conversion," in *AIP Conference Proceedings*, 1995, vol. 321, no. 1, pp. 29–43.

[5] Y. Adachi, "Compact TPV Generation System Using Al2O3/Er3Al5O12 Eutectic Ceramics Selective Emitters," in *AIP Conference Proceedings*, 2004, vol. 738, no. 1, pp. 198–205.

[6]   A. S. Vlasov, V. P. Khvostikov, O. A. Khvostikova, P. Y. Gazaryan, S. V. Sorokina, and V. M. Andreev, "TPV Systems with Solar Powered Tungsten Emitters," in *AIP Conference Proceedings*, 2007, vol. 890, no. 1, pp. 327–334.

[7]   A. Datas and C. Algora, "Development and experimental evaluation of a complete solar thermophotovoltaic system," *Progress in Photovoltaics: Research and Applications*, p. n/a–n/a, Apr. 2012.

[8]   D. Chubb, *Fundamentals of Thermophotovoltaic Energy Conversion (Google eBook)*. Elsevier, 2007, p. 530.

[9]   I. Celanovic, F. O'Sullivan, M. Ilak, J. Kassakian, and D. Perreault, "Design and optimization of one-dimensional photonic crystals for thermophotovoltaic applications," *Optics Letters*, vol. 29, no. 8, p. 863, Apr. 2004.

[10]   V. Rinnerbauer, S. Ndao, Y. X. Yeng, W. R. Chan, J. J. Senkevich, J. D. Joannopoulos, M. Soljačić, and I. Celanovic, "Recent developments in high-temperature photonic crystals for energy conversion," *Energy & Environmental Science*, vol. 5, no. 10, p. 8815, Sep. 2012.

[11]   W. R. Chan, P. Bermel, R. C. N. Pilawa-Podgurski, C. H. Marton, K. F. Jensen, J. J. Senkevich, J. D. Joannopoulos, M. Soljacic, and I. Celanovic, "Toward high-energy-density, high-efficiency, and moderate-temperature chip-scale thermophotovoltaics.," *Proceedings of the National Academy of Sciences of the United States of America*, vol. 110, no. 14, pp. 5309–14, Apr. 2013.

[12]   D. G. Gritton and R. C. Bourke, "Radioisotope-photovoltaic energy conversion system," *Advanced Energy Conversion*, vol. 5, no. 2, pp. 119–145, Jul. 1965.

[13]   V. D. Rumyantsev, "Structural Features of a Solar TPV System," in *AIP Conference Proceedings*, 2004, vol. 738, no. 1, pp. 79–87.

[14]   Z.-P. Yang, L. Ci, J. A. Bur, S.-Y. Lin, and P. M. Ajayan, "Experimental observation of an extremely dark material made by a low-density nanotube array.," *Nano letters*, vol. 8, no. 2, pp. 446–51, Feb. 2008.

[15]   W. Chan, R. Huang, C. Wang, J. Kassakian, J. Joannopoulos, and I. Celanovic, "Modeling low-bandgap thermophotovoltaic diodes for high-efficiency portable power generators," *Solar Energy Materials and Solar Cells*, vol. 94, no. 3, pp. 509–514, Mar. 2010.

[16]   A. Rabl, "Radiation transfer through specular passages—a simple approximation," *International Journal of Heat and Mass Transfer*, vol. 20, no. 4, pp. 323–330, Apr. 1977.

7   Copyright © 2013 by ASME